
Article:
Jin, L, Lee, RMA and Robertson, I (2014) Analysis and design of a novel low-loss hollow substrate integrated waveguide. IEEE Transactions on Microwave Theory and Techniques, 62 (8). pp. 1616-1624. ISSN 0018-9480

https://doi.org/10.1109/TMTT.2014.2328555

Analysis and Design of a Novel Low-Loss Hollow Substrate Integrated Waveguide

Lukui Jin, *Student Member, IEEE,* Razak Lee, *Student Member, IEEE,* and Ian Robertson, *Fellow, IEEE*

***Abstract*—In this paper, a novel hollow substrate integrated waveguide (HSIW) is presented, for realizing low-loss millimetre-wave (mm-wave) transmission lines embedded in multi-chip modules. A new analysis method for the HSIW is proposed by treating it as a combination of a two-dielectric loaded RWG and standard SIW, where an effective dielectric constant, ϵ_e, is introduced. An HSIW prototype in the Ka-band is fabricated using a progressive-lamination LTCC technique. The measured results agree well with theoretical calculations and simulations. An average of 0.009 dB/mm loss is achieved in Ka-band, which is comparable to an air-filled RWG. This shows that the technique has great potential for further development to realise highly-integrated millimetre-wave modules.**

***Index Terms*—Millimetre wave circuits, transmission lines, multichip modules.**

I. Introduction

In wireless communications, the ever increasing demand for a higher data rate and network capacity has always been a challenge for electronic engineers to address. One way is to shift the operating frequency band higher into mm-waves, such as the Ka-band used for "5G" mobile communication [1]–[3], or the 60 GHz band used for a high-definition (HD) wireless personal area network (WPAN) [4]–[7]. The successful exploitation of the millimetre-wave bands requires a cost-effective technology which can integrate Si/SiGe integrated circuits with other specialist active devices and low loss passive components on a single substrate.

A leading candidate for realizing low-loss millimetre-wave components is the substrate integrated waveguide (SIW) [8]. In 1998, two groups of Japanese researchers proposed a new type of waveguide under the name of "laminated waveguide" [9] or "post-wall waveguide" [10]. After that, Wu *et al*. introduced and theoretically analysed SIW, extracting the complex propagation constant of each SIW mode and providing basic design rules in 2002 [11] and 2005 [12]. Wu then proposed the Substrate Integrated Circuit (SIC) concept [13] and this led to intense worldwide research activity into SIW and its applications. Antennas [14], [15], filters [16], [17], mixers [18], couplers [19], circulators [20], phase shifters [21], power amplifiers [22], and power dividers [23] have all been reported using SIW embedded in a host substrate. Almost every type of microwave component has been implemented in the form of SIW, but relatively few attempts have been made to reduce the loss considerably.

Most of the research published on SIW components has been at frequencies below the mm-wave band. One reason for this is that traditional PCB technology is most often used and the resulting SIW is often too lossy for mm-wave applications. Alternatively, when SIW is realized in other mainstream fabrication technologies, such as low temperature co-fired ceramic (LTCC) and semiconductor ICs, the relatively high dielectric constant will often make the width of the SIW shrink to a size impossible for practical use at mm-waves.

Although SIW components retain many merits, such as easy fabrication, low loss, and high level of integration, *etc.*, achieving loss comparable to traditional hollow waveguide beyond 30 GHz proves to be a big problem [8].

This paper presents a novel hollow SIW (shortened to HSIW, not to be confused with HMSIW - the half-mode SIW [24]) fabricated with a progressive-lamination LTCC technology [25], with the aim of achieving much lower loss

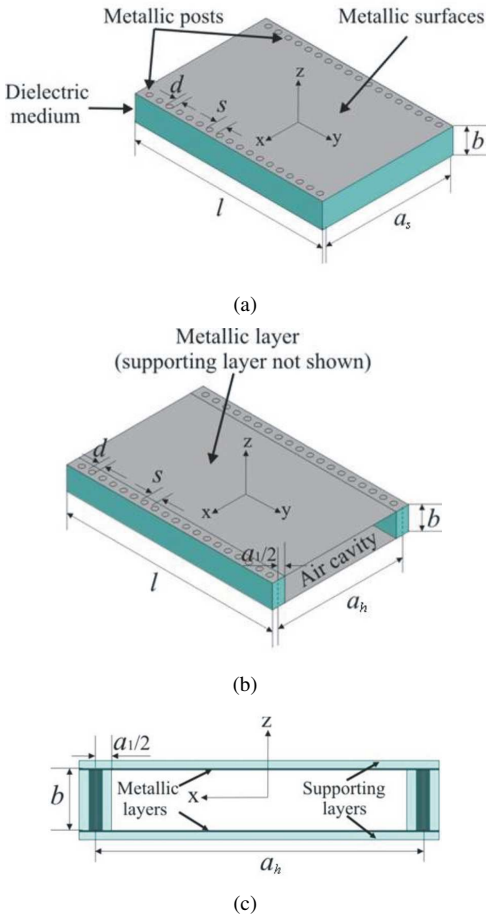

Fig. 1. The configurations of the SIW and HSIW: (a) 3D view of SIW, (b) 3D view of SIW, and (c) cross-sectional view of HSIW.

Manuscript received 13 November, 2013

L. Jin, R. Lee, and I. Robertson are all with the School of Electronic and Electrical Engineering, University of Leeds, Leeds, LS2 9JT, United Kingdom.

than the standard SIW. The HSIW is realized by removing the inner dielectric of an SIW and, hence, it incorporates a hollow cavity inside. This generates a list of advantages over the standard SIW:

1) The HSIW can be realized with high-permittivity substrates and at higher frequencies, where the size of SIW otherwise tends to be too small to be practically used.
2) Lower loss due to the removal of most of the lossy dielectric material.
3) The HSIW can be directly connected with normal RWGs as long as their heights are roughly equal, whereas the SIW requires more complicated transitions with potentially more loss.
4) The low effective dielectric constant resulting from the air cavity facilitates radiation and thus the design of high performance antennas.

Fig. 1 compares the configuration of the SIW and HSIW. Extra dielectric supporting layers are added on the top and bottom of the HSIW to support the metallic layers after the removal of inner dielectric, as shown in Fig. 1(c). To facilitate the fabrication process, the supporting layers can use the same material as the the main body of the HSIW.

The theoretical analysis method of the HSIW is a combination of that of for RWG and SIW; therefore, to analyse and design the HSIW (to find the width of the HSIW), two steps need to be followed. Firstly, the HSIW is viewed as a two-dielectric loaded RWG with the same cutoff frequency and filling dielectric. After solving this boundary value problem, the width of this RWG can be obtained and, furthermore, this RWG is transformed into a uniformly-filled RWG by introducing an effective dielectric constant (EDC), ϵ_e. Then, by modifying the empirical formula in [12] relating SIW and RWG, the width of the HSIW can finally be determined. This is described in Section II and III, respectively. In Sections IV, V, and VI, an HSIW prototype resembling WR28 is designed, fabricated, and measured to verify the theory.

II. Two-Dielectric Loaded RWG

This section deals with the boundary value problem of the two-dielectric loaded RWG to determine its width for a prescribed cutoff frequency. Firstly, by applying Maxwell's Equations with the boundary conditions, the characteristic equations for both even- and odd-modes propagating inside the RWG are set up. Then, the width of the two-dielectric loaded RWG operating in the fundamental TE_{10} mode is determined through either exact or empirical methods. Finally, an effective dielectric constant, ϵ_e, is introduced to transform the two-dielectric loaded RWG into a uniform one.

A. Characteristic Equations

As shown in Fig. 2, a metallic RWG is longitudinally filled with two symmetrical dielectrics and hence divided into three regions: 1, 2, and 3. a, b are the width and height of the two-dielectric loaded RWG, respectively, while the widths of Dielectric 1 and 2 are represented by $2a_1$ and $2a_2$, respectively. Then, it is assumed both dielectrics are linear, isotropic, homogeneous and lossless with permittivities and permeabilities

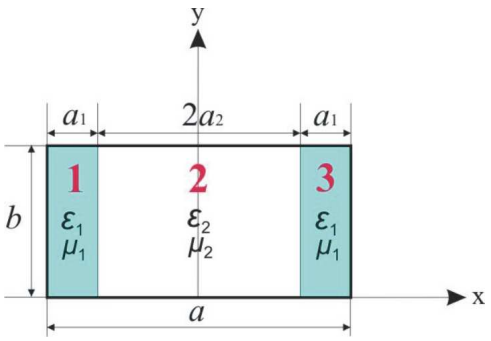

Fig. 2. The cross-sectional view of the two-dielectric loaded RWG.

of ϵ_1, μ_1 and ϵ_2, μ_2, respectively. The metal encompassing the dielectrics is assumed to be perfectly electric conductor (PEC), since the attenuation due to a finite conductivity and a lossy dielectric will not affect the propagation characteristics much in a low-loss situation [26], [27].

A simple odd/even-mode method is used to analyse the two-dielectric loaded RWG on the basis that the fields within it are either symmetrical or asymmetrical, $i.e.$, even or odd with respect to the plane of $x = 0$, since the RWG is symmetrical in terms of material and geometry with respect to the same plane. The final results of the characteristic equations following the method in [28] are found as follows:

Even mode,

$$\left[\frac{K_\mu k_{x1}\tan(k_{x1}a_1)}{k_{c1}^2}-\frac{k_{x2}}{k_{c2}^2\tan(k_{x2}a_2)}\right]\left[\frac{K_\epsilon k_{x1}}{k_{c1}^2\tan(k_{x1}a_1)}-\frac{k_{x2}\tan(k_{x2}a_2)}{k_{c2}^2}\right]+\left(\frac{\beta c_2 n\pi}{\omega b}\right)^2\left(\frac{1}{k_{c2}^2}-\frac{1}{k_{c1}^2}\right)^2=0, \tag{1}$$

and odd mode,

$$\left[\frac{K_\mu k_{x1}\tan(k_{x1}a_1)}{k_{c1}^2}+\frac{k_{x2}\tan(k_{x2}a_2)}{k_{c2}^2}\right]\left[\frac{K_\epsilon k_{x1}}{k_{c1}^2\tan(k_{x1}a_1)}+\frac{k_{x2}}{k_{c2}^2\tan(k_{x2}a_2)}\right]+\left(\frac{\beta c_2 n\pi}{\omega b}\right)^2\left(\frac{1}{k_{c2}^2}-\frac{1}{k_{c1}^2}\right)^2=0, \tag{2}$$

where $K_\mu = \mu_1/\mu_2$, $K_\epsilon = \epsilon_1/\epsilon_2$, c_2 is the speed of light in Dielectric 2, and k_{x1}, k_{x2} satisfies the following separation equation:

$$\begin{aligned}\epsilon_r k_0^2 &= k_{x1}^2 + (n\pi/b)^2 + \beta^2\\ k_0^2 &= k_{x2}^2 + (n\pi/b)^2 + \beta^2\end{aligned} \tag{3}$$

B. TE_{10} Mode

A special case of the propagating modes inside the two-dielectric loaded RWG when $n = 0$ should be mentioned here. If $n = 0$, the longitudinal electric component, E_z, vanishes, generating TE_{m0} modes. It can then be derived that the TE_{10} mode is fundamental when $b/a \leq 1$ which is the case for regular RWGs [28].

Now we assume that Dielectric 2 is air and Dielectric 1 is a nonmagnetic material with a relative permeability, $\mu_r = 1$, and a relative permittivity, ϵ_r. Then, $K_\mu = 1$ and $K_\epsilon = \epsilon_r$.

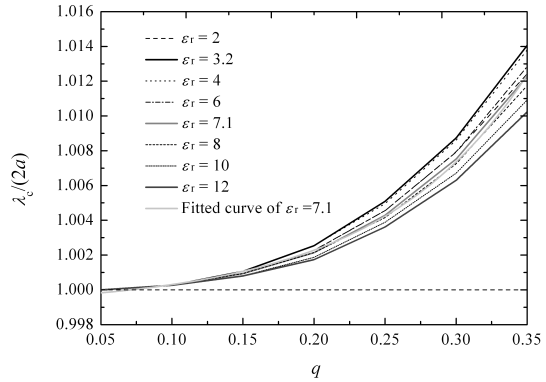

Fig. 3. The comparison of cutoff wavelength with different dielectric constants and the curve fitting.

To determine the cutoff frequency of the TE_{10} mode which has a symmetrical distribution of transverse electric fields and hence belongs to the even-mode group, we set β in (3) to 0, which then reduces (1) to

$$\sqrt{\epsilon_r}k_0a_1 = \arctan\left[\sqrt{\epsilon_r}/\tan\left(k_0a_2\right)\right] + m'\pi \tag{4}$$

where $m' = 0, 1, 2, \cdots$

Note, in this equation, there are four unknowns, a, p, ϵ_r, and k_0. With three of them given, the remaining one can be solved for immediately. This, in another perspective, offers a high degree of flexibility when designing the two-dielectric loaded RWG.

If k_0 is the target, then when it has been worked out, the cutoff frequency can be derived as:

$$f_c = \frac{k_0 c_0}{2\pi} \tag{5}$$

where c_0 is the speed of light in free space. It is also worth noting that m' has nothing to do with m. In fact, when m' takes one single value, it could correspond to a series of continuous guided modes depending on the number of curve intersections represented by the two sides of (4).

Since the HSIW has most of its inner dielectric removed and behaves like an air-filled RWG, the dielectric-loaded RWG considered here should also be lightly loaded, *i.e.*, either $2a_1/a$ or $\sqrt{\epsilon_r}$ or the product of them is small. So, a new loading ratio, q, is defined as:

$$q = \frac{2a_1\sqrt{\epsilon_r}}{a} \tag{6}$$

to characterise a dielectric-loaded RWG. The lower q is, the closer the RWG behaves to its air-filled counterpart.

For those lightly-loaded RWGs with q up to 0.35, a series of different dielectric constants has been used to theoretically calculate the accurate cutoff frequency through (4), as shown in Fig. 3. The relative dielectric constant ϵ_r starts at 2 and ends at 12 with a step of 2. Generally, when ϵ_r increases, the normalised cutoff wavelength λ_c decreases and it behaves more like the TE_{10} mode of an air-filled RWG. However, note that the maximum λ_c doesn't appear at the lowest ϵ_r, as it resembles, again, an air-filled RWG when ϵ_r approaches 1. It is therefore found through accurate calculation that $\epsilon_r = 3.2$ gives the maximum λ_c.

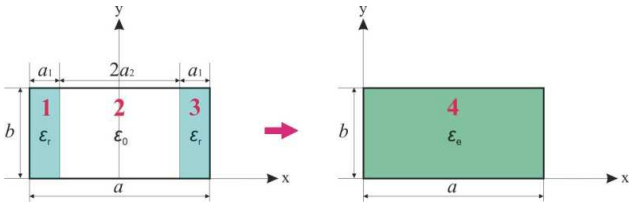

Fig. 4. The transformation from a two-dielectric loaded RWG into a uniformly filled one of EDC, ϵ_e.

Since (4) needs to be numerically calculated, which is complicated, a curve-fitting technique is used here to derive a simplified approximation. For $2 \leq \epsilon_r \leq 12$ which accounts for most of the regular dielectric materials, $\epsilon_r = 7.1$ is chosen to be curve-fitted, as it stands close to the middle and will later be used for the HSIW design. The fitted curve takes the form of an exponential function, shown as the gray solid line in the middle of the curve cluster in Fig. 3. The approximated empirical expression for the cutoff wavelength of TE_{10} mode is

$$\lambda_c = 2a\left[0.999 + 4.946 * 10\text{^}(-4)\exp\left(9.409q\right)\right],\ q \leq 0.35 \tag{7}$$

with a discrepancy less than 0.2% for $2 \leq \epsilon_r \leq 12$. After that, the cutoff frequency is obtained as:

$$f_c = \frac{c_0}{\lambda_c}. \tag{8}$$

C. EDC

Now we introduce a virtual dielectric with an EDC of ϵ_e, which completely fills the inside of the RWG, to replace the E-plane dielectric which has a relative dielectric constant of ϵ_r and a loss tangent of $\tan\delta$, as shown in Fig. 4. After the replacement, the new dielectric loaded RWG should be able to present a similar propagation characteristic, compared with the old one. Suppose the original dielectric is low loss and since

$$\epsilon = \epsilon' - j\epsilon'' = \epsilon_0\epsilon_r(1 - j\tan\delta) \tag{9a}$$

$$\epsilon_e = \epsilon'_e - j\epsilon''_e = \epsilon_0\epsilon_{re}(1 - j\tan\delta_e) \tag{9b}$$

the derivation of ϵ_e can be divided into two independent stages without affecting each other [26].

1) Derivation of ϵ_{re}: Firstly, we solve for the propagation constant, β, of the TE_{10} mode by referring to the characteristic equation (4) with a simplified separation equation:

$$\begin{aligned} \epsilon_r k_0^2 &= k_{x1}^2 + \beta^2 \\ k_0^2 &= k_{x2}^2 + \beta^2 \end{aligned} \tag{10}$$

Then, under the premise of a completely-loaded RWG, the propagation constant, β, can be rewritten as:

$$\beta = \sqrt{\epsilon_{re}k_0^2 - (\pi/a)^2} \tag{11}$$

Therefore, the real part of the EDC can be derived as:

$$\epsilon_{re} = \frac{\beta^2 + (\pi/a)^2}{k_0^2} \tag{12}$$

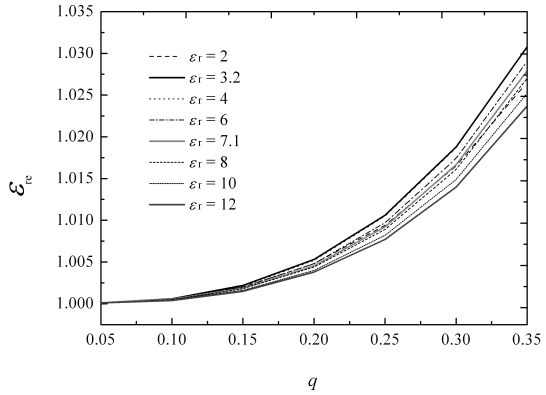

Fig. 5. The theoretically calculated ϵ_{re} of a two-dielectric loaded RWG with different ϵ_r at $f = 1.5f_c$.

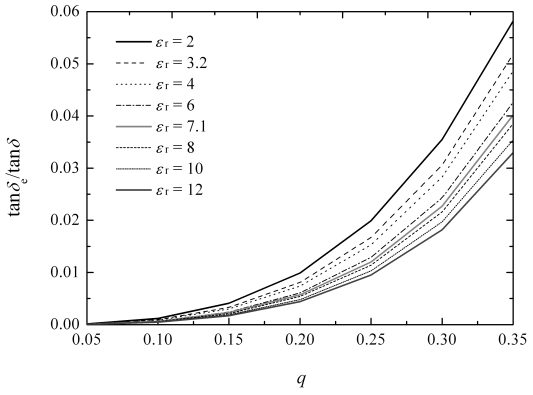

Fig. 7. The theoretical normalised $\tan\delta_e$ of a two-dielectric loaded RWG with different ϵ_r at $f = 1.5f_c$.

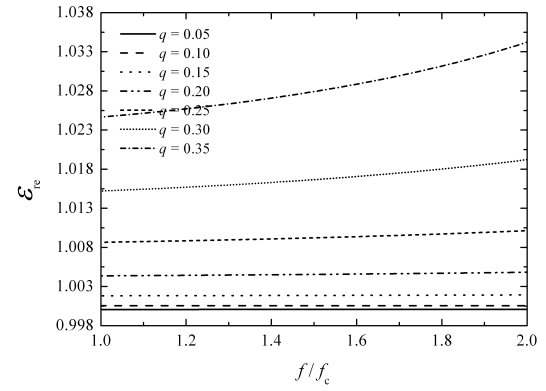

Fig. 6. The theoretically calculated ϵ_{re} of a two-dielectric loaded RWG with different q ($\epsilon_r = 7.1$).

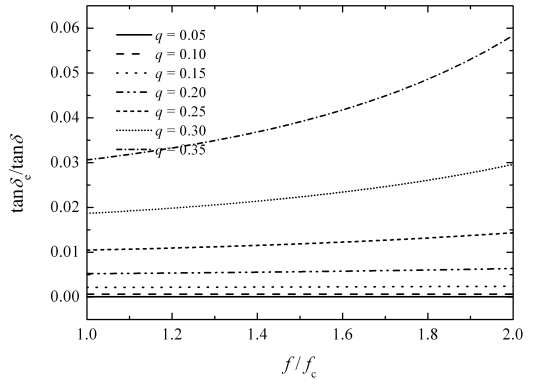

Fig. 8. The theoretical normalised $\tan\delta_e$ of a two-dielectric loaded RWG with different q ($\epsilon_r = 7.1$).

Results for a series of ϵ_r values are theoretically calculated with different loading ratio, q, at the center of the single-mode band, $i.e.$, $f = 1.5f_c$. The result is shown in Fig. 5. As can be seen, a cluster of curves, with $2 \leq \epsilon_r \leq 12$, tends to open up toward higher q values, which indicates a worse deviation. ϵ_{re} from $\epsilon_r = 7.1$ stands in the middle with the maximum deviation, 0.4%, occurring at $q = 0.35$. Note that this deviation is achieved at $f/f_c = 1.5$. As the frequency rises, the deviation is expected to be increased toward the end of the single-mode band, $f/f_c = 2$.

Next, we take $\epsilon_r = 7.1$ as an example to perform the theoretical calculation across the whole single-mode band, $i.e.$, $f_c \sim 2f_c$. The result is shown in Fig. 6. It can be seen that ϵ_{re} takes the form of an exponential function and tends to flare up with high q values in the single-mode band. To ensure a uniform dielectric, q should be kept as low as possible, preferrably below 0.3.

2) Derivation of $\tan\delta_e$*:* Following the rule of power conservation, the time-average power dissipated per unit length due to the dielectric loss of the two RWGs shown in Fig. 4 should be equal to each other. Based on this, $\tan\delta_e$ can be derived as:

$$\tan\delta_e = \frac{\epsilon_e''}{\epsilon_e'} = \frac{\epsilon_e''}{\epsilon_{re}} = \tan\delta\left(\frac{\epsilon_r}{\epsilon_{re}}\right) \left[1 + \frac{k_{x1}^2}{k_{x2}^2}\frac{2a_2 + k_{x2}^{-1}\sin(2k_{x2}a_2)}{2a_1 - k_{x1}^{-1}\sin(2k_{x1}a_1)}\frac{\cos^2(k_{x1}a_1)}{\sin^2(k_{x2}a_2)}\right]^{-1} \quad (13)$$

Similar to the analysis of ϵ_{re}, a series of ϵ_r has also been calculated to obtain $\tan\delta_e/\tan\delta$ and shown in Fig. 7. Since $\tan\delta_e/\tan\delta$ varies with changing frequency especially for a high q, a fixed frequency point at $f/f_c = 1.5$ has been chosen to evaluate it. It is seen in Fig. 7 that a cluster of curves, with $2 \leq \epsilon_r \leq 12$, tend to flare up toward higher q values, which is similar to that depicted in Fig. 5. The only difference lies in that $\tan\delta_e$ is monotonically increasing with the decrease of ϵ_r. The $\tan\delta_e$ for $\epsilon_r = 7.1$ stands in the middle with the maximum deviation, 2%, occurring at $q = 0.35$. Note that this deviation is achieved at $f/f_c = 1.5$. As the frequency rises, the deviation is expected to increase towards the edge of the single-mode band, $f/f_c = 2$.

A series of $\tan\delta_e$ normalised to the actual dielectric loss tangent, $\tan\delta$, has been calculated using (13) with different

q values, as shown in Fig. 8. Note that ϵ_r is also chosen to be 7.1, where a moderate $\tan\delta_e$ is prompted. It can be found in Fig. 8 that the curves also take the form of an exponential function and tend not to be flat with high q values in the single-mode band. To ensure a uniform dielectric, q should also be kept as low as possible, preferrably below 0.3.

III. SIW

In this section, a multimode calibration method proposed in [12] is used to analyse and extract the propagation characteristics of the SIW. After that, a modified formula based on Wu's method in [11] and [12] is given to relate SIW and its counterpart RWG.

As stated in Section I, the main difference between an SIW and a completely dielectric-filled RWG lies in that the solid side walls of a RWG are replaced by two rows of periodic metal posts. As can be seen in Fig. 1(a), the diameter of the posts is d and the pitch between two adjacent posts is s. In addition, a_s, b, and l represent the width, height, and length of the SIW, respectively. Note that a_s is defined from the centers of the metal posts, as only the dielectric within the confinement of the posts takes effect.

Based on [12], only TE_{m0} modes can propagate within an SIW, since the discrete posts will cut off the surface currents of all other modes. This is in line with the propagation of the TE_{10} mode in the two-dielectric loaded RWG. Various methods have been applied to analyse the propagation characteristics of this newly-introduced structure. By assuming a uniform longitudinal electric current on the post surface, Hirokawa $et.\ al.$ used the dyadic Green's function to solve the fields generated by a unit cell of the SIW. This method is completely numerical without giving any closed-form formula [10]. Wu has used the BI-RME method in [11], the FDTD method, and a multimode calibrated FEM method in [12]. Apart from the numerical nature of these two methods, approximated numerical formulas are derived to determine the equivalent RWG width of an SIW, which is simple and straightforward within a certain accuracy.

A. Two-Mode Calibration Method

The multimode calibrated FEM method is employed here to characterise the SIW. The multimode calibration method is essentially a multiline method, where the basic principle is that one can determine the propagation constant through uncalibrated S-parameter measurements of at least two transmission lines [29], [30]. Two lowest-order modes will be considered in our case, with HFSS simulations based on the FEM method used to implement the calculation.

B. Modified Relation between SIW and RWG

Following this two-mode calibration method, the propagation characteristics of three SIWs with different widths, $a_s = 2,\ 3$, and 4 mm are calculated and compared with results obtained from [12], while the other parameters are chosen as $b = 1$ mm, $d = 0.25$ mm, $s = 0.5$ mm, $\sigma = 3.7e7$ S/m, $\tan\delta = 0.001$, and $\epsilon_r = 7.1$ (the filling dielectric is LTCC).

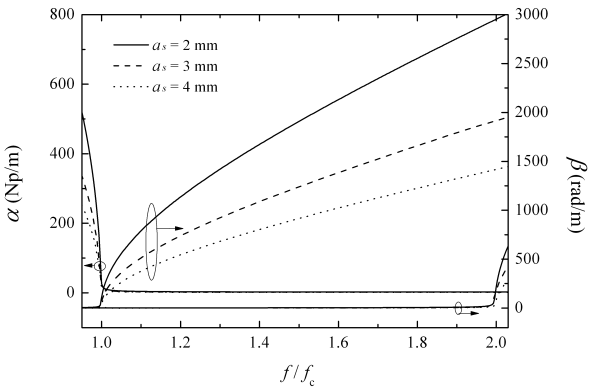

Fig. 9. The simulated attenuation constant, α and the phase constant, β of three SIWs with different widths, $a_s = 2,\ 3$, and 4 mm.

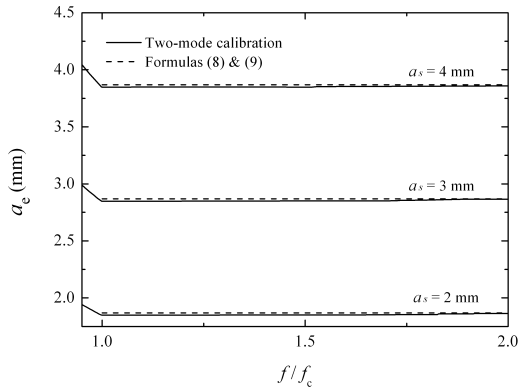

Fig. 10. The equivalent width, a_e, of three SIWs with different widths, $a_s = 2,\ 3$, and 4 mm for $\epsilon_r = 7.1$ (Formulas (8) and (9) are from [12]).

Fig. 9 shows the simulated propagation constants of the three SIWs with the frequency normalised to their own cutoff. The attenuation constant, α, is for the TE_{10} mode. Mode 2 starts to appear at $f/f_c = 2$, where the single-mode band ends. Based on the phase constant, β, of TE_{10} mode in Fig. 9, we can use

$$a_e = \frac{\pi}{\sqrt{\epsilon_r k_0^2 - \beta^2}} \tag{14}$$

to find the equivalent width of a RWG completely filled with the same dielectric material, as shown in Fig. 10.

An interesting phenomenon is discovered here that the equivalent width, a_e, is weakly increasing with the frequency and tends to merge with a constant value given by [12] at the end of the single-mode band, $i.e.$, $f/f_c = 2$ (Note that results given by Formulas (8) and (9) are overlapping each other and thus, presented in one curve). Therefore, a maximum discrepancy is indicated at the cutoff frequency, $i.e.$, $f/f_c = 1$. In an ideal situation, the definition of the cutoff is where the phase constant, β, equals 0. In the HFSS simulation, however, β takes a small positive value below the cutoff. Therefore, the new definition of the cutoff is where the largest leap of β happens, which is also where a_e stops dropping and tends to

TABLE I
THE EQUIVALENT WIDTH, a_e, FROM TWO-MODE CALIBRATION METHOD AND WU'S METHOD [12] FOR $\epsilon_r = 7.1$.

a_s (mm)	2	3	4
a_e (mm, Formula (8) in [12])	1.868	2.868	3.868
a_e (mm, two-mode calibration)	1.847	2.847	3.848

TABLE II
THE EQUIVALENT WIDTH, a_e, OF THE SIW WITH $a = 3$ MM FROM TWO-MODE CALIBRATION METHOD FOR DIFFERENT ϵ_r.

ϵ_r	2	4	6	8	10	12
a_e (mm)	2.837	2.838	2.852	2.843	2.847	2.840

be flat in Fig. 10. To accurately determine the cutoff frequency, a_e at $f/f_c = 1$ is required.

The a_e from both two-mode calibration method and [12] is shown in Table I. A maximum discrepancy of 1.1% can be observed. Apparently, however, Formula (8) will match our results if the coefficient of the second term is adjusted slightly as:

$$a_e = a_s - \frac{d^2}{0.817 \cdot s} \tag{15}$$

In order to find out whether ϵ_r plays a role or not in determining the equivalent width, a_e, the SIWs of $a = 3$ mm with different ϵ_r are analysed. Results are shown in Table II. As can be seen, the influence of ϵ_r is minor and has no obvious trend, which means that ϵ_r is not a determining factor to derive a_e and the small deviations among different ϵ_r might be attributed to insufficient simulation accuracy.

Other basic design rules with respect to s/d and a_s/d in [12] can be followed to minimise the leakage loss, ensure a proper TE_{m0} mode, *etc.*

IV. HSIW

The typical context in which a single-mode HSIW needs to be designed is that the material, fabrication technology, and cutoff frequency have all been specified and the dimensions of the HSIW need to be determined. As stated before, the HSIW is viewed as a combination of a two-dielectric loaded RWG and an SIW. With the introduction of ϵ_e, the RWG is transformed into a uniformly-filled one and hence, (14) and (15) are rewritten as:

$$a_e = \frac{\pi}{\sqrt{\epsilon_{re} k_0^2 - \beta^2}} = a_h - \frac{d^2}{0.817 \cdot s} \tag{16}$$

to determine the width of the HSIW. Note that to ensure a frequency-invariant ϵ_{re} and thus a_e, the loading ratio, q, needs to be close to 0 or $\sqrt{\epsilon_r}$. Otherwise, a_e varies with frequency, which means that this type of HSIW cannot be characterized by a two-dielectric loaded RWG of a constant width. Since our HSIW has removed most of the dielectric, it well satisfies the condition. Therefore, by combining the analysis in Sections II and III, a general rigorous design procedure of the HSIW can be obtained as follows:

1) Decide the cutoff frequency f_c of the TE_{10} mode and hence, the single-mode band is $f_c \sim 2f_c$.
2) Determine s, d, a_1, and ϵ_r based on the materials and techniques available and make sure $s/d \leq 2$, $2a_1/d \geq 1$.
3) Use (4) to find the width of the two-dielectric loaded RWG, a, for f_c and check if $a/d \geq 5$. If not, reduce d, or a_1 until it satisfies the condition. Numerical analysis is needed to solve this transcendental equation.
4) Use (16) to find the width of the HSIW, a_h. Note that $a_e = a$. The height of the HSIW, b, enjoys a certain degree of flexibility and can be selected according to the convenience of fabrication, loss requirements, *etc.*
5) Use the two-mode calibration method to find the propagation characteristics, *i.e.*, α and β. HFSS based on the FEM method is needed to perform the 3D modelling.

Based on the steps discussed above, an HSIW has been designed in the Ka-band which has the same cutoff frequency as the standard WR28 (21.10 GHz). The Dupont™ GreenTape™ 9K7 LTCC system as mentioned before has been employed as the dielectric material, with $\epsilon_r = 7.1$ and $\tan\delta = 0.001$ at 10 GHz. The conductivity of the silver paste to be coated on the LTCC is $\sigma = 3.7\mathrm{e}7$ S/m.

Table III shows the structural parameters of the WR28-like HSIW, where a_r is the width of a standard RWG. The propagation characteristics are shown in Fig. 11, where the frequency has been normalised to the simulated cutoff. Standard WR28 and a corresponding dielectric-filled SIW with the same cutoff frequency have also been simulated by HFSS and results are shown for comparison. Note that the height of the RWG and SIW is also 1 mm, the same as the HSIW.

In Fig. 11(a), the loss of SIW indicated by the attenuation constant, α, is significantly larger than that of the HSIW. This has clearly verified the reduction of loss by removing the inner dielectric of the SIW. Compared with the standard RWG, the WR28-like HSIW is very close to a standard waveguide in terms of attenuation, which shows we achieved the design goal.

In Fig. 11(b), the phase constants, β, of the HSIW and WR28 for the TE_{10} mode are almost overlapping each other and the cutoff frequency defined by the largest derivative of β is only 0.11 GHz discrepancy. For the TE_{20} mode, however, that deviation doubles and can be observed in Fig. 11(b). The SIW, in contrast, has a similar cutoff frequency; while the rate of increase of β is far higher than that of the other two structures.

TABLE III
THE STRUCTURAL PARAMETERS (IN MM) OF THE WR28-LIKE HSIW.

a_r	a_1	a	a_h	b	d	s
7.11	0.70	7.08	7.26	1	0.30	0.60

V. FABRICATION

The WR28-like HSIW designed in Section IV was fabricated with a progressive-lamination LTCC technology without the use of sacrificial materials [31]. The material is, as stated

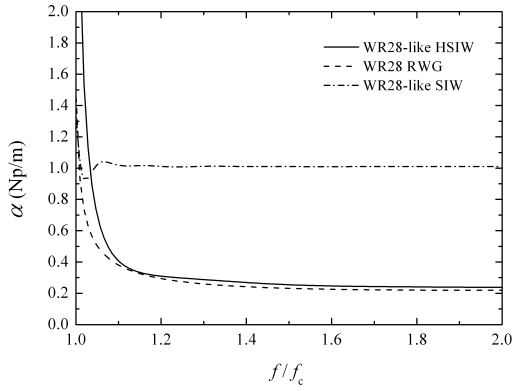

(a)

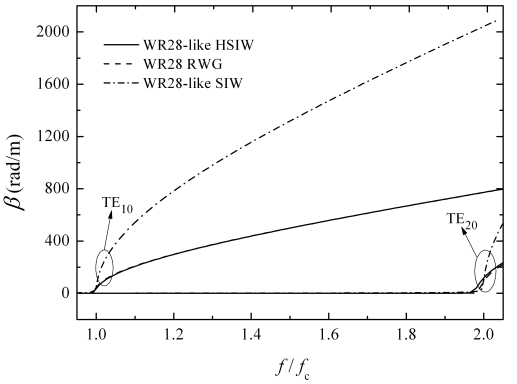

(b)

Fig. 11. The propagation characteristics of the WR28-like HSIW in contrast with the corresponding RWG and SIW: (a) the attenuation constant, α; (b) the phase constant, β.

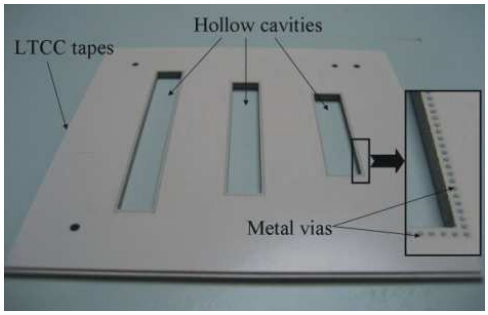

Fig. 12. The middle layers of LTCC tape before lamination of the top and bottom.

in previous sections, Dupont^{TM} GreenTape^{TM} 9K7, the single-layer thickness of which is 0.254 mm before firing. In total, there are four middle layers where the cavity and via-hole sidewalls are laser machined, as shown in Fig. 12, and 2 supporting layers at the top and bottom to support the metallic layers of the upper and lower broadwalls. The fabrication procedure is as follows:

1) Pre-lamination: All the raw LTCC sheets need be pre-laminated at 20 MPa, 70°C for 10 min to provide sufficient densification for minimizing the shrinkage. Note that the 4 middle layers are pressed together, while the top and bottom supporting layers are done so individually.
2) Laser-machining: A Nd:YAG laser machine (ProtoLaser 200 from LPKF^{TM}) is used to cut out shapes and structures, such as vias, slots, cavities, $etc.$
3) Screen-printing: The LL601 paste for via filling and LL612 paste for layer metalisation were deposited onto the LTCC samples with an Aurel VS1520A screen printer.
4) Lamination: All layers were then aligned using a jig and laminated using a uniaxial laminator.
5) Co-firing: The stacked green tapes were then co-fired using a programmable furnace according to a temperature profile for around 36.5 hours.

The manufactured HSIW test samples are shown in Fig. 13(a). Three HSIWs with an equal difference in length of 10 mm, $i.e.$, 30 mm, 40 mm, and 50 mm, are built into one tape. This saves time, material, and facilitates the application of the two-mode calibration method presented in Section III.

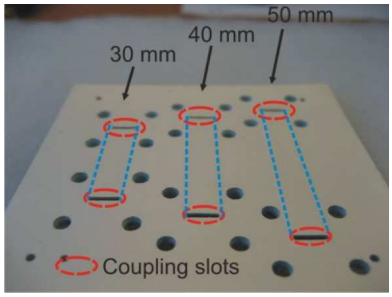

(a)

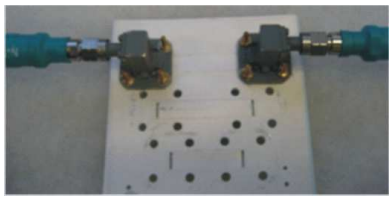

(b)

Fig. 13. (a) The prototype of the WR28-like HSIW and (b) its measurement fixture.

VI. Measurement

As shown in Fig. 13, a back-to-back transversal slot-pair is employed to couple the energy in and out. Around each slot, there are also four holes to mount the RWG-to-Coax adaptor, as shown in Fig. 13(b). To verify this feeding scheme, the measured and simulated S-parameters of the 30 mm HSIW are shown in Fig. 14. It can be seen that they agree well.

Through the multimode calibration technique, the propagation constant of this WR28-like HSIW can be extracted, and is shown in Fig. 15. To compare with results from the measurement, the simulated propagation constant using HFSS has also been plotted in the same figure.

In Fig. 15, the measured phase constant, β, stays very close to the simulated one, including around the cutoff frequency. As for the measured loss constant, α, it ripples above the

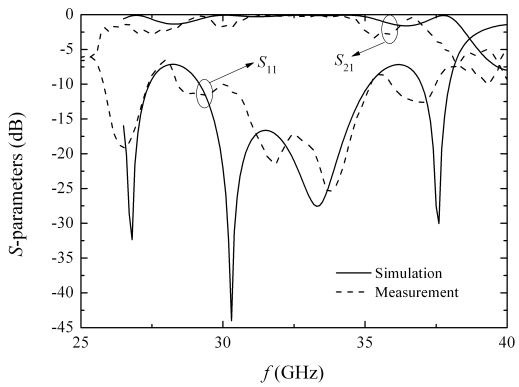

Fig. 14. Measured and simulated S-parameters of the 30-mm-long HSIW.

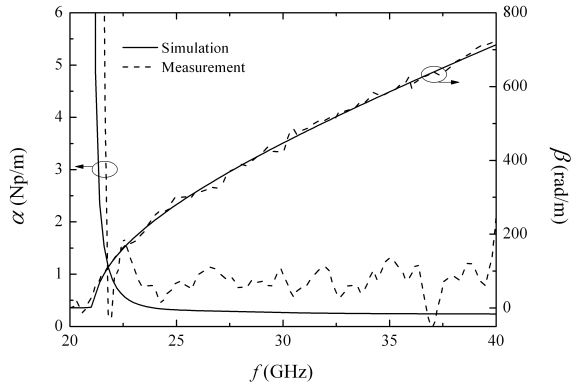

Fig. 15. Extracted attenuation constant, α and phase constant, β of the WR28-like HSIW from the measurement.

simulated one, which indicates that the actual sample is more lossy. Possible reasons may lie in that the loss characteristics of materials (LTCC, silver paste) tend to be worse at high frequencies; in particular, in this experimental in-house process we have observed significant surface roughness issues and some voids in the fired silver paste, which will certainly deteriorate the loss performance of the HSIW. Even with these fabrication issues, an average α of approximately 1 Np/m or 9 dB/m is still achieved, which is an excellent loss performance. Furthermore, we are confident that these fabrication issues could be addressed with suitable process optimization in a commercial environment.

VII. Conclusion

By decomposing the HSIW into the two-dielectric loaded RWG and a standard SIW, this paper develops a systematic method for the analysis and design of the hollow SIW (HSIW). A prototype operating in Ka-band has been fabricated using an experimental progressive lamination method of fabricating LTCC channels and the measured results suggest that the HSIW can achieve transmission loss comparable to a standard RWG with the same cutoff frequency. The potential for HSIW to be integrated with other active and passive components in an integrated multilayer, multi-chip module is highly attractive and the technology offers tremendous prospects for realizing low-loss integrated passive components such as resonators, filters, power combiners and antennas.

Acknowledgment

The authors wish to acknowledge the financial support of the University of Leeds FIRS Scholarship scheme and Ministry of Education Malaysia SLAB Scholarship. This work was partly supported by the EPSRC project "3D Microwave & Millimetre-Wave System-on-Substrate using Sacrificial Layers for Printed RF MEMS Component" which is in collaboration with Loughborough University and Imperial College London.

References

[1] L. Garber, "News briefs," *Computer*, vol. 46, no. 8, pp. 18–20, 2013.

[2] T. Rappaport, S. Sun, R. Mayzus, H. Zhao, Y. Azar, K. Wang, G. Wong, J. Schulz, M. Samimi, and F. Gutierrez, "Millimeter wave mobile communications for 5G cellular: It will work!" *IEEE Access*, vol. 1, pp. 335–349, 2013.

[3] H. Zhao, R. Mayzus, S. Sun, M. Samimi, J. K. Schulz, Y. Azar, K. Wang, G. N. Wong, F. J. Gutierrez, and T. S. Rappaport, "28 GHz millimeter wave cellular communication measurements for reflection and penetration loss in and around buildings in New York city," in *IEEE International Conference on Communications (ICC)*, 2013, pp. 5163–5167.

[4] P. Smulders, "Exploiting the 60 GHz band for local wireless multimedia access: prospects and future directions," *IEEE Communications Magazine*, vol. 40, no. 1, pp. 140 –147, Jan. 2002.

[5] M. Peter, W. Keusgen, and J. Luo, "A survey on 60 GHz broadband communication: Capability, applications and system design," in *European Microwave Integrated Circuit Conference*, Oct. 2008, pp. 1–4.

[6] P. X. Su-Khiong (SK) Yong and A. V. Garcia, Eds., *60 GHz Technology for Gbps WLAN and WPAN: From Theory to Practice*. John Wiley & Sons, Ltd, 2011.

[7] G. de Alwis and M. Delahoy, "60 GHz band millimetre wave technology," Spectrum Planning and Engineering Team, Radiofrequency Planning Group, Australian Communications Authority, Tech. Rep., 2004.

[8] M. Bozzi, A. Georgiadis, and K. Wu, "Review of substrate-integrated waveguide circuits and antennas," *IET Microwaves, Antennas Propagation*, vol. 5, no. 8, pp. 909–920, 2011.

[9] H. Uchimura, T. Takenoshita, and M. Fujii, "Development of a 'laminated waveguide'," in *IEEE MTT-S International Microwave Symposium Digest*, vol. 3, 1998, pp. 1811–1814.

[10] J. Hirokawa and M. Ando, "Single-layer feed waveguide consisting of posts for plane TEM wave excitation in parallel plates," *IEEE Transactions on Antennas and Propagation*, vol. 46, no. 5, pp. 625 – 630, 1998.

[11] Y. Cassivi, L. Perregrini, P. Arcioni, M. Bressan, K. Wu, and G. Conciauro, "Dispersion characteristics of substrate integrated rectangular waveguide," *IEEE Microwave and Wireless Components Letters*, vol. 12, no. 9, pp. 333–335, Sept. 2002.

[12] F. Xu and K. Wu, "Guided-wave and leakage characteristics of substrate integrated waveguide," *IEEE Transactions on Microwave Theory and Techniques*, vol. 53, no. 1, pp. 66 – 73, 2005.

[13] K. Wu, D. Deslandes, and Y. Cassivi, "The substrate integrated circuits - a new concept for high-frequency electronics and optoelectronics," in *Telecommunications in Modern Satellite, Cable and Broadcasting Service*, vol. 1, Oct. 2003, pp. III–X.

[14] B. Sanadgol, S. Holzwarth, A. Milano, and R. Popovich, "60 GHz substrate integrated waveguide fed steerable LTCC antenna array," in *Proceedings of the Fourth European Conference on Antennas and Propagation (EuCAP)*, 2010, pp. 1–4.

[15] K. Wu, Y. J. Cheng, T. Djerafi, X. P. Chen, N. Fonseca, and W. Hong, "Millimeter-wave integrated waveguide antenna arrays and beamforming networks for low-cost satellite and mobile systems," in *Proceedings of the Fourth European Conference on Antennas and Propagation (EuCAP)*, 2010, pp. 1–5.

[16] D. Stephens, P. Young, and I. Robertson, "Millimeter-wave substrate integrated waveguides and filters in photoimageable thick-film technology," *IEEE Transactions on Microwave Theory and Techniques*, vol. 53, no. 12, pp. 3832 – 3838, 2005.
[17] Y. Cheng, W. Hong, and K. Wu, "Design of a substrate integrated waveguide modified R-KR lens for millimetre-wave application," *IET Microwaves, Antennas & Propagation*, vol. 4, no. 4, pp. 484 – 491, 2010.
[18] Z. Zhen-Yu, K. Wu, and N. Yang, "A millimeter-wave sub-harmonic self-oscillating mixer using dual-mode substrate integrated waveguide cavity," *IEEE Transactions on Microwave Theory and Techniques*, vol. 58, no. 5, pp. 1151 – 1158, 2010.
[19] B. Liu, W. Hong, Y.-Q. Wang, Q.-H. Lai, and K. Wu, "Half mode substrate integrated waveguide (HMSIW) 3-db coupler," *IEEE Microwave and Wireless Components Letters*, vol. 17, no. 1, pp. 22 – 24, 2007.
[20] W. D'Orazio and K. Wu, "Substrate-integrated-waveguide circulators suitable for millimeter-wave integration," *IEEE Transactions on Microwave Theory and Techniques*, vol. 54, no. 10, pp. 3675 – 3680, 2006.
[21] K. Sellal, L. Talbi, T. Denidni, and J. Lebel, "Design and implementation of a substrate integrated waveguide phase shifter," *IET Microwaves, Antennas and Propagation*, vol. 2, no. 2, pp. 194 – 199, 2008.
[22] M. Abdolhamidi, M. ; Shahabadi, "X-band substrate integrated waveguide amplifier," *IEEE Microwave and Wireless Components Letters*, vol. 18, no. 12, pp. 815 – 817, 2008.
[23] D.-S. Eom, J. Byun, and H.-Y. Lee, "Multilayer substrate integrated waveguide four-way out-of-phase power divider," *IEEE Transactions on Microwave Theory and Techniques*, vol. 57, no. 12, pp. 3469 – 3476, 2009.
[24] W. Hong, B. Liu, Y. Wang, Q. Lai, H. Tang, X.-X. Yin, Y.-D. Dong, Y. Zhang, and K. Wu, "Half mode substrate integrated waveguide: A new guided wave structure for microwave and millimeter wave application," in *Infrared Millimeter Waves and 14th International Conference on Teraherz Electronics*, Sept 2006, pp. 219–219.
[25] D. Jurkow, H. Roguszczak, and L. Golonka, "Cold chemical lamination of ceramic green tapes," *Journal of the European Ceramic Society*, vol. 29, no. 4, pp. 703 – 709, 2009.
[26] D. M. Pozar, *Microwave Engineering*, 3rd ed. Wiley India Pvt. Limited, 2009.
[27] R. Seckelmann, "Propagation of TE modes in dielectric loaded waveguides," *IEEE Transactions on Microwave Theory and Techniques*, vol. 14, no. 11, pp. 518–527, Nov. 1966.
[28] J. van Bladel and T. J. Higgins, "Cut-off frequency in two-dielectric layered rectangular wave guides," *Journal of Applied Physics*, vol. 22, no. 3, pp. 329 –334, Mar. 1951.
[29] R. Marks, "A multiline method of network analyzer calibration," *IEEE Transactions on Microwave Theory and Techniques*, vol. 39, no. 7, pp. 1205–1215, Jul. 1991.
[30] M. Janezic and J. Jargon, "Complex permittivity determination from propagation constant measurements," *IEEE Microwave and Guided Wave Letters*, vol. 9, no. 2, pp. 76–78, Feb. 1999.
[31] M. F. Shafique, A. Laister, M. Clark, R. E. Miles, and I. D. Robertson, "Fabrication of embedded microfluidic channels in low temperature co-fired ceramic technology using laser machining and progressive lamination," *Journal of the European Ceramic Society*, vol. 31, no. 13, pp. 2199–2204, 2011.

Lukui Jin (S'12) received both his B.S. and M.S. degree in microwave engineering from Harbin Institute of Technology, Harbin, China, in 2008 and 2010, respectively. After that, he went to study in University of Leeds, UK, and received his Ph.D. degree also in microwave engineering in 2014.

He is one of the 9 award holders of Leeds Fully-funded International Research Scholarship in 2010. His current research interests include design and analysis of substrate integrated waveguide, dielectric waveguide, and their applications in antennas and filters in the MCM technology.

Razak Mohd Ali Lee (S'10) received both his B.Eng. and M.Eng. from Nagaoka University of Technology, Niigata, Japan, in 1999 and 2001, respectively. In 2001, he joined Tokyo Electron Limited, Tokyo, Japan, where he was a Field Engineer, then at the same year moved to Plasma Etching System Development and Manufacturing Centre at Tokyo Electron Yamanashi, Yamanashi, Japan. In 2006, he joined the School of Engineering and Information Technology, University Malaysia Sabah as a Lecturer. In 2014, he received his Ph.D degree in the University of Leeds, Leeds, United Kingdom.

His research interests involve multilayered-microwave device fabrication and its miniaturization techniques on LTCC and thick-film technology and integrated waveguides.

Ian Robertson.jpg (M'96- SM' 05 -Fellow 12) was born in London in 1963. He received his BSc (Eng) and PhD degrees from King's College London in 1984 and 1990, respectively. From 1984 to 1986 he worked in the MMIC Research Group at Plessey Research (Caswell). After that he returned to King's College London, initially as a Research Assistant and then as a Lecturer, finally becoming Reader in 1994. In 1998 he was appointed Professor of Microwave Subsystems Engineering at the University of Surrey, where he established the Microwave Systems Research Group and was a founder member of the Advanced Technology Institute.

He has organized many colloquia, workshops, and short courses for both the IEE and IEEE. He was the Honorary Editor of IEE Proceedings - Microwaves, Antennas & Propagation for many years and Editor-in-Chief of the rebranded IET Microwaves, Antennas & Propagation from 2005 to 2009. He edited the book 'MMIC Design' published by the IEE in 1995 and co-edited the book RFIC & MMIC Design and Technology, published in English 2001 and in Chinese in 2007. He has published over 400 papers in the areas of MIC and MMIC design. In June 2004 he was appointed to the University of Leeds Centenary Chair in Microwave and Millimetre-Wave Circuits and he is now Head of the School of Electronic & Electrical Engineering.